Composites Part B 176 (2019) 107078

Contents lists available at ScienceDirect

Composites Part B

journal homepage: www.elsevier.com/locate/compositesb

Reinforcing carbon fiber epoxy composites with triazine derivatives functionalized graphene oxide modified sizing agent

Lichun Ma [a,*], Yingying Zhu [a], Peifeng Feng [a], Guojun Song [a], Yudong Huang [b], Hu Liu [c,**], Jiaoxia Zhang [d,e], Jincheng Fan [f], Hua Hou [g], Zhanhu Guo [d]

[a] Institute of Polymer Materials, College of Chemistry and Chemical Engineering, Qingdao University, Qingdao, 266071, China
[b] School of Chemical Engineering and Technology, Harbin Institute of Technology, Harbin, 150001, China
[c] Key Laboratory of Materials Processing and Mold (Zhengzhou University), Ministry of Education, National Engineering Research Center for Advanced Polymer Processing Technology, Zhengzhou University, Zhengzhou, 450002, China
[d] Integrated Composites Laboratory (ICL), Department of Chemical & Biomolecular Engineering, University of Tennessee, Knoxville, TN, 37996, USA
[e] School of Materials Science and Engineering, Jiangsu University of Science and Technology, Zhenjiang, 212003, China
[f] College of Materials Science and Engineering, Changsha University of Science and Technology, Changsha, 410114, China
[g] School of Materials Science and Engineering, North University of China, Taiyuan, 030051, China

ARTICLE INFO

Keywords:
Graphene oxide
Carbon fibers
Polymer-matrix composites
Interfacial strength

ABSTRACT

To improve the dispersion of graphene oxide (GO) nanosheets in sizing agent and to enhance the interfacial adhesion between GO and epoxy, GO nanosheets were chemically modified with cyanuric chloride (TCT) and diethylenetriamine (DETA). The functionalized GO (i.e. GO-TCT-DETA) with different contents was introduced into the carbon fiber (CF) interface by sizing process. The uniform distribution of GO sheets on CF surface and the enhancement of surface roughness were obtained. Moreover, significant enhancements (i.e., 104.2%, 100.2%, and 78.3%) of interfacial shear strength (IFSS), interlaminar shear strength (ILSS), and flexural properties were achieved in the composites with only 1.0 wt% GO-TCT-DETA sheets introduced in the fiber sizing. The GO-TCT-DETA in the interface region enhanced the stress being transferred effectively and the local stress concentrations being relieved. This study indicates that the utilization of functionalized GO is one of the alternative approaches for controlling the fiber-matrix interface and improving the mechanical properties of CF epoxy composites.

1. Introduction

Carbon fibers (CFs) reinforced polymer composites with high specific strength, great corrosion resistance, light-weight, and favorable design flexibility are superseding the conventional metal and ceramic materials in a variety of high-performance structural and functional applications, such as aerospace, automotive, industries, sports and so on [1–13]. The performance of fiber-reinforced composites highly depends on the fiber-matrix interface, a prominent interface can guarantee the efficient stress transfer from the weaker matrix to the stronger fiber, which is conducive to reduce stress concentrations and to improve overall mechanical properties [14–16]. However, stress concentration and crack formation in the interfaces can deteriorate the properties of the composites. Consequently, the surface modification of CFs to develop an excellent interphase is pivotal for improving the performance of composites [17].

Recently, multiscale reinforcement has attracted substantially technical and commercial interests in developing fibers reinforced polymer composites [18]. The deposition of nanoparticles onto the CF surface enhanced significantly the interfacial performance by availably augmenting the fiber surface area, and facilitating mechanical interlocking and local stiffening at the interface region [19–25]. Many approaches have been reported to attach nanoparticles to the fiber surface including chemical vapor deposition (CVD) [26], chemical grafting [27,28], electrophoretic deposition (EPD) [29,30], nanoparticles modified sizing agents etc. Compared with the above reported methods, nanoparticles modified sizing agent possesses unique simplicity and flexibility and is suitable for large-scale industrial production [31]. Additionally, the attachment of nanoparticles onto the CF surface sized with a polymer coating could not only form a connected network structure at the

* Corresponding author.
** Corresponding author.
E-mail addresses: malcqdu@163.com, mlc@qdu.edu.cn (L. Ma), liuhu@zzu.edu.cn (H. Liu).

https://doi.org/10.1016/j.compositesb.2019.107078
Received 8 April 2019; Received in revised form 19 May 2019; Accepted 1 July 2019
Available online 4 July 2019

interface to restrain the movement of polymer chains and boost mechanical interlocking as well as affinity with matrix for improving the stress transfer, but also protect greatly the fiber surface and improve the tensile strength of fibers [32]. For example, Wu et al. [33] reported over 46.5% improvement of interlaminar shear strength (ILSS) in a CF/methylphenylsilicone resin (MPSR) composites when the CNTs were introduced in the fiber sizing and the tensile strength of sized CFs showed a slight increase.

In recent years, incorporation of typical two-dimensional graphene or graphene oxide (GO) sheets has been demonstrated to increase the strength of polymer and to improve the interfacial properties of fiber reinforced composites [34–36]. However, poor dispersion and agglomeration of graphene or GO in media are the great obstacles and causes nano defects in the interface region and only minimal enhancement of interfacial properties was achieved [37–39]. Therefore, efforts to figure out the factors that influence the composites interfacial properties and to achieve superior enhancement in the interfacial strength are significant and urgent targets.

Low-cost diethylenetriamine (DETA) possesses unique polar characteristics with a mixture of primary, secondary amines groups. It can not only react with GO but also be used as curing and toughening agent for epoxy matrix [40–44]. Cyanuric chloride (CTC) has a triazine ring with stable chemical nature and three active reaction sites of chlorine atoms, and can act as a main tree trunk to construct amine dendrimers [45]. Compared with other polymers or natural products [46–52], this dendritic compound contains a mixture of primary, secondary and tertiary amines groups. Thus, they are interesting from the perspective for providing a range of active sites to react with epoxy resin [53,54]. If GO surface is covalently functionalized by low-cost triazine derivatives with terminal-amine groups, it would provide an ambient path for strong bonding with epoxy matrix and high dispersion in matrix. The effects of triazine derivatives functionalized GO sizing on the interfacial properties of CF/epoxy resin composites have not been reported yet.

In this work, the GO nanosheets were chemically modified with cyanuric chloride (TCT) and diethylenetriamine (DETA) and then dispersed in the fiber sizing agent. The modified sizing agent was directly deposited on the CF surface. The effects of sizing agent containing GO and modified GO on the interfacial microstructure, interfacial adhesion strength, and flexural property of CF composites were studied and discussed in details.

2. Materials and methods

2.1. Materials

PAN-based CFs (7 mm in diameter) were bought from Sino steel Jilin Carbon Co., China. Bisphenol A epoxy resins (E51) and liquid aromatic diamine (H-256) were used as matrix and hardening agent. Natural graphite was obtained from Qingdao Tianhe Co., Ltd. Potassium permanganate ($KMnO_4$), sodium nitrate ($NaNO_3$), triethylamine (TEAE), lithium aluminum hydride ($LiAlH_4$), methylene chloride, TCT and DETA were purchased from Fengxian Tianjin, China (Qigang Rd, Tianjin). H_2O_2, THF, H_2SO_4 and HCl were obtained from Tianjin, China. All reagents were analytical grade.

2.2. Chemical functionalization of GO

GO was prepared using a modified Hummers method [43]. The aim of chemical functionalization was to produce more amine-containing functional groups on the GO surface. Firstly, GO was impregnated in saturated $LiAlH_4$-THF solution for 2 h to obtain GO-OH. Then, TCT and TEAE were added to the mixture containing GO-OH and THF and stirred for 24 h at 70 °C to obtain GO-TCT. Then, the GO-TCT was dispersed in methylene chloride through ultrasonic for 1.5 h. Finally, the hybrid of DETA and NaOH (mass ratio of 1: 2) was appended to the above solution at 80 °C and sustained for 12 h [55] to acquire DETA functionalized GO-TCT, labeled as GO-TCT-DETA. The grafting course of TCT and DETA onto GO was described in Fig. 1.

2.3. Preparation of sizing agents including GOs and CF/epoxy composites

Primarily, the commercial CFs were desized in acetone at 80 °C for 48 h to remove the polymer sizing and pollutants [55], and were defined as untreated CFs. The extracted CFs were conducted with $AgNO_3$ (0.01 mol/L)/$K_2S_2O_8$ (0.1 mol/L) solution at 343 K for 1 h to generate carboxylic groups (CF–COOH). Then, quantitative GO-TCT-DETA was added into epoxy/toluene solution with a GO-TCT-DETA content of 0.1, 0.5, 1.0 and 1.5 wt%, and the hybrid was stirred for 30 min, the sizing resin was maintained constantly at 1.5 wt% in the fiber sizing. The sizing agents including virgin GO were also acquired by the identical way. The CFs were plucked under a traction by a nip roller using a customized small-scale sizing line, then crossed a sizing dip bath including various GOs-processed sizing agents, and by subsequent drying them in a drying oven. The pulling speed of CFs was maintained gently enough to ensure good wetting and to realize the superfluous resin to be eliminated. At last, the sized CFs were conserved in dryer for future use.

The unidirectional prepreg of CFs and epoxy resin (EP) was fit into a mold to prepare composites by using the molding technique, the epoxy resin (E−51) and curing agent (H-256) were uniformly mixed in a mass ratio of 100: 32. Briefly, the composites were fabricated by heating the samples at 90 °C for 2 h without pressure, and pressurized to 5 MPa, heating up to 120 °C for 2 h, followed by curing at 150 °C for 3 h. The CF content in composites was maintained in the range of 60 ± 1.5%. The whole preparation courses of the sized CFs and CF/epoxy composites are exhibited in Fig. 2.

2.4. Characterizations

The surface structure and chemical composition of functionalized GOs were measured by FTIR spectrophotometer (NEXUS), X-ray photoelectron spectroscopy (XPS, ESCALAB 220i-XL), X-ray diffraction (XRD, DX-2700) and Raman spectrometer (RM2000). The structures and topographic characteristics of functionalized GO were detected by scanning electron microscope (SEM, JSM-7800F) and transmission electron microscopy (TEM, G2F30).

Dynamic contact angle meter (DCAT21, Germany) was carried out to detect the dynamic contact angle of fiber surface. Deionized water and diiodomethane were used as the test liquids. The polar and dispersive components could be obtained through Equation (1):

$$\gamma_l(1+\cos\theta) = 2(\gamma_l^p\gamma_f^p)^{\frac{1}{2}} + 2(\gamma_l^d\gamma_f^d)^{\frac{1}{2}} \quad (1)$$

$$\gamma_f = \gamma_f^p + \gamma_f^d \quad (2)$$

where γ_l, γ_l^d and γ_l^p are the surface tension of the test liquid, and its dispersive and polar components, respectively.

The monofilament debonding test (FA620, Japan) was utilized to analyze the interfacial shear strength (IFSS) between the CFs and epoxy resin. The microdroplets were prepared by the mixture of E−51 and H-256 at a weight ratio of 100:32. The fiber was pulled out from the cured resin and the value of IFSS was calculated depending on Formula (3):

$$IFSS = \frac{F}{\pi dl} \quad (3)$$

where F was the recorded load, d was the CF diameter, and l was the embedded length with resin. The recorded value of IFSS for each group of specimens was averaged from the data of 50 successful measurements.

The interlaminar shear strength (ILSS) of the CFs/epoxy resin composites was analyzed by a three-point short beam shear test according to ASTM D2344. The value of ILSS was calculated according to Equation

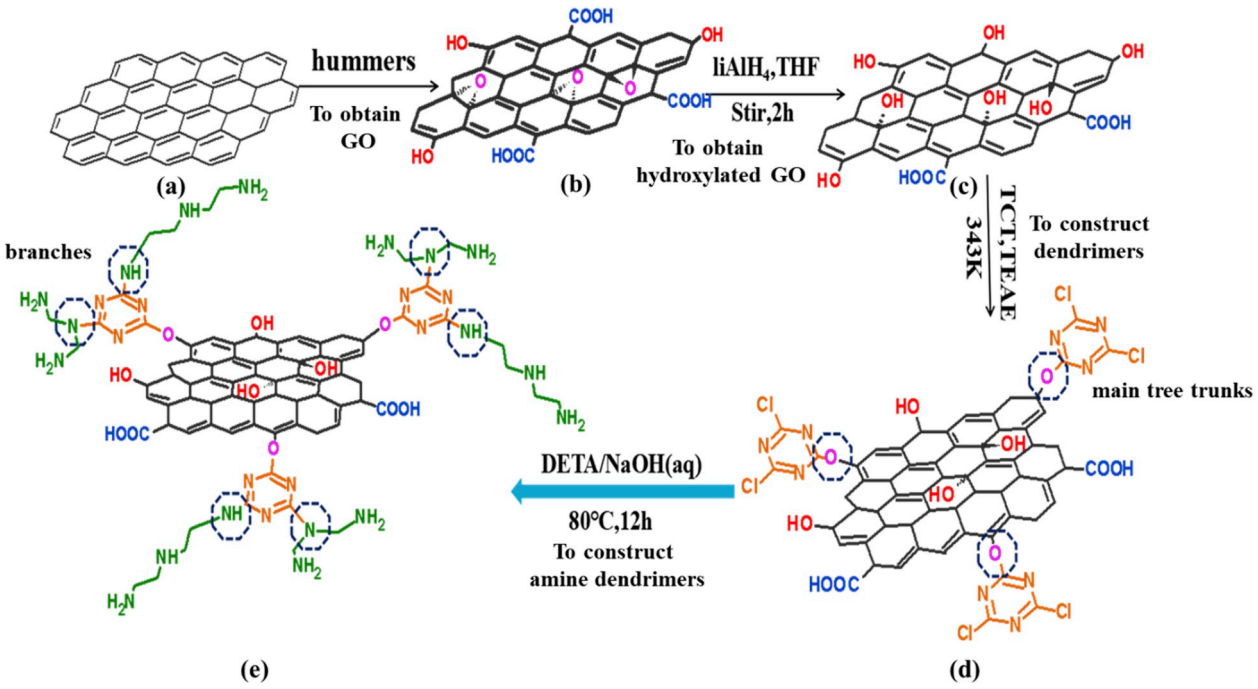

Fig. 1. Schematic illustration of GO functionalized with TCT-DETA: (a) Nature graphite, (b) GO, (c) GO-OH, (d) GO-TCT, (e) GO-TCT-DETA.

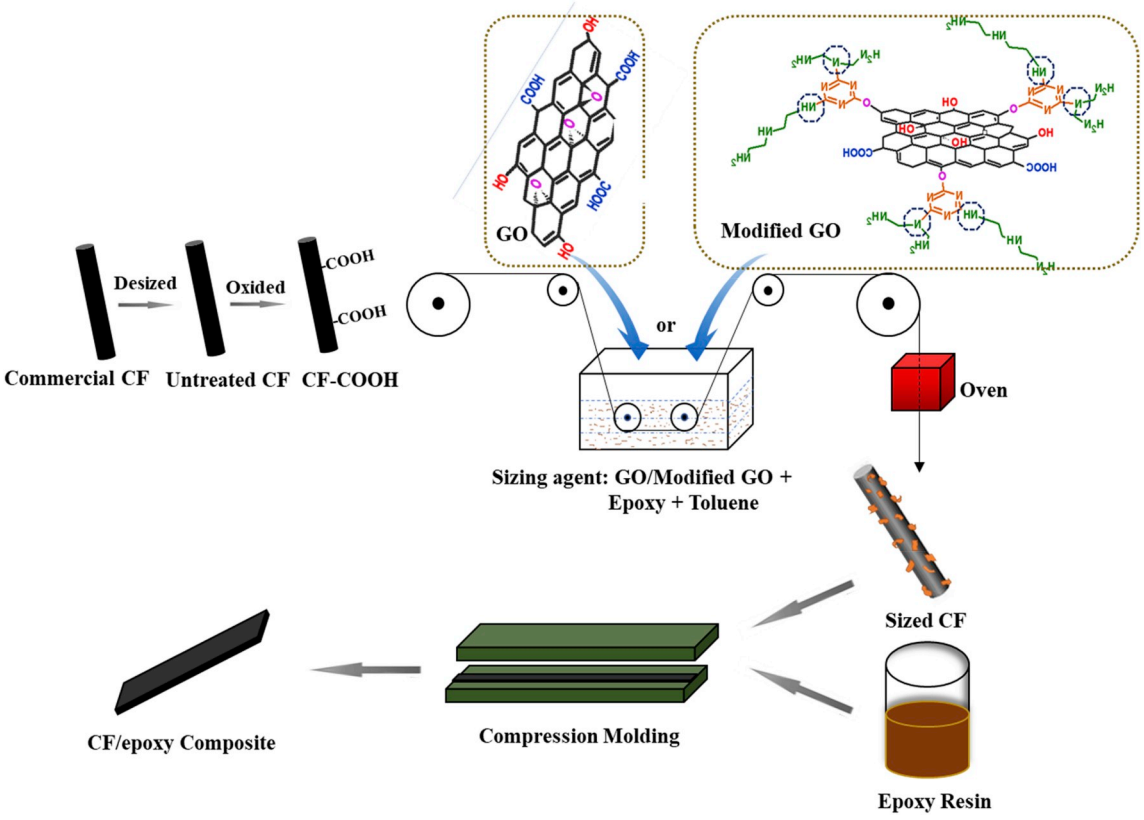

Fig. 2. The diagrammatic drawing of sizing process including GOs and composites preparation.

(4):

$$ILSS = \frac{3F_{max}}{4bh} \quad (4)$$

where F_{max} represents the maximum compression load recorded (N), b was the width (mm) and h was the thickness (mm) of specimen. All the presented results were an average of five specimens.

Flexural tests were carried out by a three-point bending mode and conducted on GT-7000-A2X (Taiwan, China) with a crosshead speed of 2 mm min^{-1} according to GB/T 9341-2008. The sample size was

60 mm × 6 mm × 2 mm. All the presented results were an average of five specimens. The value of flexural strength (σ) was calculated according to Formula (5):

$$\sigma = \frac{3FL}{2bh^2} \tag{5}$$

where F was the maximum load recorded (N), L was the sample span (mm), b was the width (mm) and h was the thickness (mm) of specimen.

The morphology and roughness (R_a) of CF surface were tested by atomic force microscopy (AFM, NT-MDT Co., Russia) and field-emission scanning electron microscopy (FESEM, Quanta 200FEG, Japan).

3. Results and discussion

3.1. Characterizations of the GO

The GO modified with TCT and DETA was analyzed by FTIR, as displayed in Fig. 3a. For virgin GO, the absorption peaks at 1039, 1608, 1716 and 3100 cm^{-1} were assigned to C–O–C, C═C, C═O and –OH from carboxyl, respectively [43]. In the spectrum of GO-OH, the absorption peak at 3388 cm^{-1} was from the O–H strengthening and the intensity of C═O was decreased greatly, which was due to the reduction of GO by $LiAlH_4$. For GO-TCT, two broad peaks at 1714 and 1568 cm^{-1} were attributed to the vibration absorption of triazine ring skeleton, and the signal peak at 826 cm^{-1} was assigned to the -C-Cl of TCT, indicating that

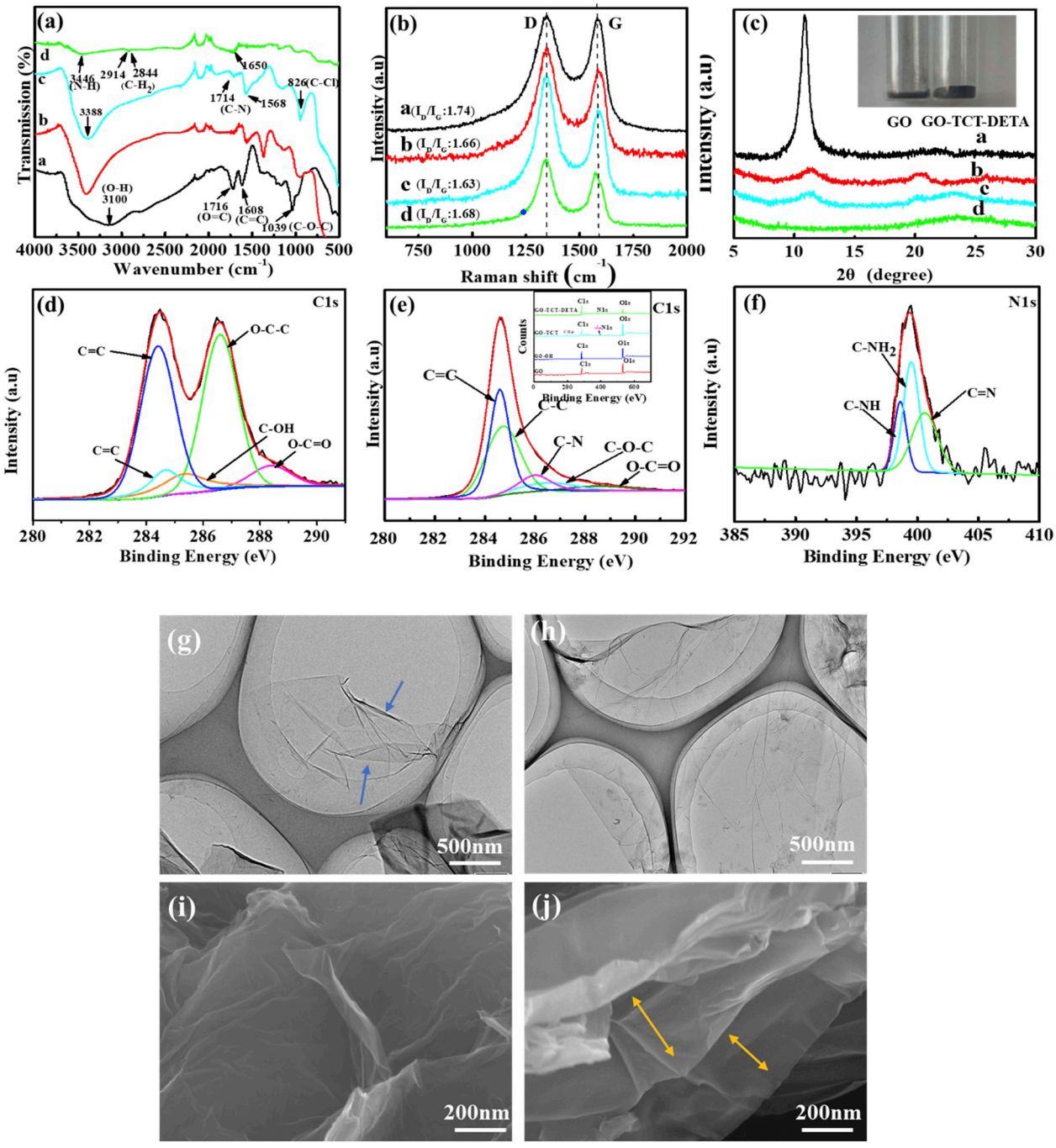

Fig. 3. FTIR spectra (a), Raman spectra (b), XRD curves (d) and C1s XPS spectra (d) GO, (e) GO-TCT-DETA and N1s XPS spectra of GO-TCT-DETA and TEM and SEM images of (g, i) GO and (h, j) GO-TCT-DETA.

TCT had been grafted onto the GO surface. After grafting DETA, the peak of C–Cl vanished and new peaks at 1650 and 3446 cm^{-1} appeared, attributing to the vibration and stretching of N–H bond. The peaks at 2844 and 2914 cm^{-1} were assigned to C–H (-CH_2) from DETA, testifying the reaction between chlorine (Cl) on GO-TCT and amide groups (-NH_2) on DETA [44]. Therefore, TCT and DETA had been covalently attached onto the GO surface.

Raman spectroscopy was adopted to further characterize the surface structures of the functionalized GO, as displayed in Fig. 3b. The value of I_D/I_G of virgin GO was 1.74, after TCT modification, the I_D/I_G value of GO-TCT was reduced to 1.63, which might be because that the stable six heterocyclic rings in TCT had made up for the sp^2 of GO [45]. The I_D/I_G value of GO-TCT-DETA increased to 1.68, which was still less than that of GO. The consequences demonstrated that the covalent grafting of triazine derivatives did not severely destroy the GO carbon lattice.

The exfoliation of virgin GO and modified GO was analyzed by XRD, as exhibited in Fig. 3c. The peak value of GO at 10.85° reflected that the layer spacing of graphene was 0.82 nm. After modified by TCT-DETA, GO-TCT-DETA displayed a broad diffraction peak at 8.3°, testifying the increased interlayer spacing (1.09 nm). This manifested that the grafted GO nanosheets with triazine derivatives were stacked together by an incompact manner. Furthermore, the inset illustration revealed different volumes for GO and GO-TCT-DETA with the identical weight, which was consistent with the result of XRD, indicating that the interlayer spacing of GO-TCT-DETA was greater than that of GO due to the reaction chains by interspersing among GO layers.

The surface chemical composition of GO and GO-TCT-DETA was determined by XPS, as presented in Fig. 3d–f. For GO, the binding energy (B.E.) of C1s at 284.6 eV and O1s at 531.9 eV appeared and the contents of C and O were 59.61% and 40.39%, respectively. After grafting TCT and DETA, the Cl2p peak at 197.7 eV vanished and the N1s peak at 399.4 eV showed a little increase from 2.18% to 5.30%, which implied the reaction occurred between the chlorine in TCT and amine groups in DETA. The functional groups on the GO surfaces were estimated by the peak fitted C1s and N1s spectra. The C1s spectrum of GO (Fig. 3d) displayed peaks at 288.6, 286.7 and 285.3 eV, respectively, which were attributed to the O–C═O, C–O–C and C–OH produced on the GO via modified Hummers method. In the case of GO-TCT-DETA (Fig. 3e), the disappearance of C–Cl peak and the improvement of C–N contents testified that TCT and DETA were already adhered onto the GO surface, which was further identified with the results of FTIR and Raman. The chemical reaction of TCT and DETA with GO was further verified by N1s, as exhibited in Fig. 3f. Three extra peaks at 399.6, 398.5 and 398.1 eV appeared and were attributable to primary, secondary and tertiary amine (C–NH_2, C–NH and C–N) [56], which also proved the chemical reaction between DETA and GO-TCT.

The microstructures and topographies of GO and GO-TCT-DETA sheets were observed through TEM and SEM, as revealed in Fig. 3(g-j). The TEM image shows that the GO sheets displayed a diameter of a few micrometers and some wrinkles. After covalent functionalization, the GO-TCT-DETA surface had some ramifications and folds, which were assigned to the triazine derivative chains grafted on the GO. Moreover, it also showed commendable exfoliation and great dispersion, which was in accordance with the XRD results.

The GO surface was slick and homogeneous from Fig. 3i, but the accumulation was more serious and formed a three-dimensional layer. While the surface and edge of GO-TCT-DETA displayed more wrinkles (Fig. 3j), which were resulted from the augmented interlayer spacing through grafting branching chains onto the GO surface, and interlayer structure was slacker than that of GO. Two GO sheets could be linked together to produce a crosslinking of the GO layer by DETA with two terminated amine groups [57]. Moreover, the functionalization to GO by triazine derivative did not generate a prominent damage for the sp^2 structures of GO sheets, which was in line with a mild rise in the I_D/I_G value in Raman analysis as discussed.

3.2. Surface topography of CFs

The CF surface topographies after sizing GO or GO-TCT-DETA with different ratios were observed by SEM and AFM, as shown in Fig. 4. It was noted that the shallow grooves on CF surface had been filled up by a layer of resin-containing GO or GO-TCT-DETA, but some big bulges of GO could be observed in Fig. 4b, mainly due to the GO agglomeration resulted from the poor dispersibility of GO in the epoxy sizing agent system even at a low concentration (0.5 wt%), this might affect the degree of interfacial enhancement. Fig. 4c–f presents the surface morphologies of CFs sized by sizing agent with different concentrations of GO-TCT-DETA (0.1, 0.5, 1.0 and 1.5 wt%). With increasing the GO-TCT-DETA content from 0.1 to 1.0 wt%, the number of GO-TCT-DETA deposited on CF surface increased, and could cover the entire CF surfaces homogeneously, as seen in Fig. 4c–e. More and more contact points were created and thus enhanced the mechanical interlocking to stiffen the interface of the resulting composites. However, much higher content of GO-TCT-DETA (such as 1.5 wt%) resulted in the agglomeration of GO during the film formation and the nonuniformity on the CF surface (Fig. 4f), which could cause concentrated regional stress and reduced energy dissipation ability, leading to less effective interfacial enhancement of composites.

3.3. Dynamic contact angle (DCA) analysis

DCA tests were carried out to examine the effects of sizing agent containing GO or GO-TCT-DETA on the surface energy. The results are summarized in Table 1. In comparison with untreated CF, the surface free energy of CF-GO 0.5 increased to 49.22 mN m^{-1} from 30.56 mN m^{-1} owing to the introduced GO sheets with oxygen-containing functional groups and high specific surface area. For CF-GO-TCT-DETA 0.1, the contact angles were found more distinctly decreasing, decreased to 51.98° for polar water and 45.37° for non-polar diiodomethane, respectively. Furthermore, the surface energy, its dispersion and polar components obviously increased compared with CF-GO 0.5, which was resulted from a better dispersion of GO-TCT-DETA on fiber surface and externally introduced amino-terminated groups. Moreover, with increasing the content of GO-TCT-DETA from 0.1 to 1.0 wt%, the surface energy was enhanced evidently from 55.04 mN m^{-1} for CF-GO-TCT-DETA 0.1–67.78 mN m^{-1} for CF-GO-TCT-DETA 1.0, however, the increased amplitude of CF-GO-TCT-DETA 1.5 was decreased due to the reduction in polarity groups caused by the agglomeration of excess GO sheets. A higher surface energy could give rise to a superior wettability particularly, which was propitious to the improvement of the interfacial properties of the composites.

3.4. Mechanical property evaluation of CF/epoxy composites

3.4.1. Interfacial property of CF/epoxy composites

The effect of the sizing layer with GO sheets on the interfacial performance of CF/epoxy composites was examined by IFSS. The results are presented in Fig. 5. The IFSS of CF-GO/epoxy composites (62.2 MPa) had a small increase (25.4%) in comparison with untreated CF/epoxy composites (49.6 MPa). The sizing with GO introduced on the CF surfaces increased the surface roughness and played an important role in enhancing the interfacial strength, but the GO agglomeration and the weak wettability as well as inferior chemical bonding between GO and epoxy resin confined the improvement of IFSS effectively.

For CF-GO-TCT-DETA reinforced resin composites, the GO sheets surrounding the CFs with the help of triazine derivatives contributed to the improvement of IFSS. The IFSS results of CF-GO-TCT-DETA composites were much higher than those of untreated CF and CF-GO composites, especially CF-GO-TCT-DETA1.0 composites yielding an IFSS of 101.3 MPa, which gave rise to a 104.2% and 62.9% improvement in comparison to untreated CF and CF-GO composites. The improvement of IFSS was mainly ascribed to the increased fiber surface area and the

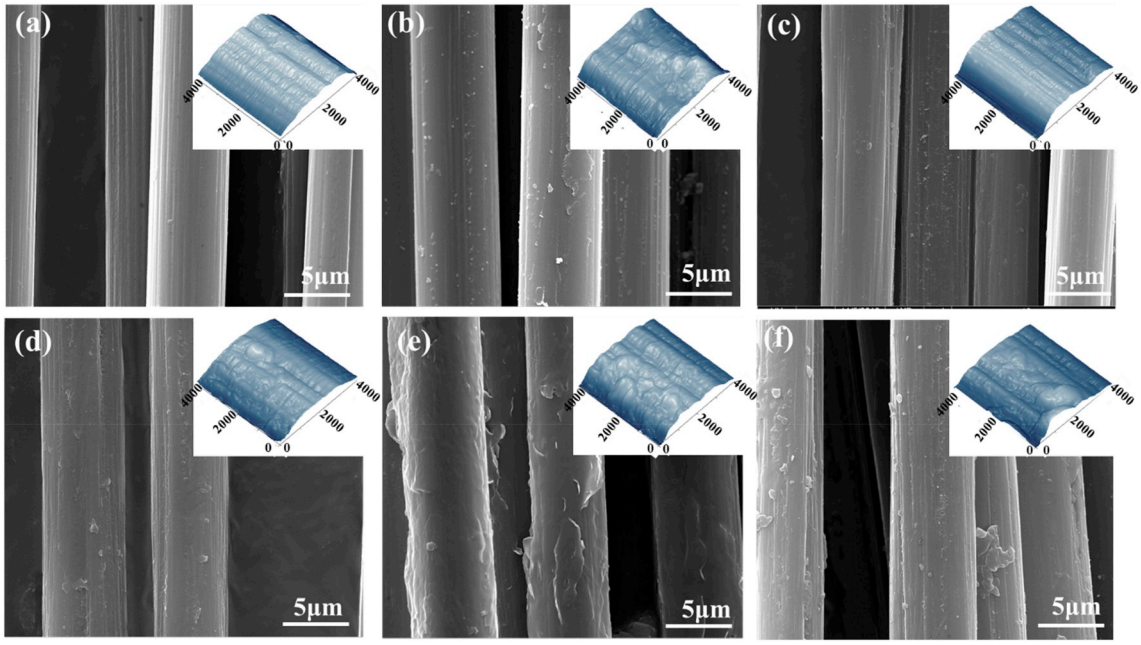

Fig. 4. SEM images of (a) untreated CFs, (b) CF-GO 0.5, (c) CF-GO-TCT-DETA 0.1, (d) CF-GO-TCT-DETA 0.5, (e) CF-GO-TCT-DETA 1.0 and (f) CF-GO-TCT-DETA 1.5.

Table 1
Contact angles and surface energy of CFs.

Samples	Contact angles (°)		Surface energy ($mN{\cdot}m^{-1}$)		
	θ_{water}	$\theta_{diiodomethan}$	γ^d	γ^p	γ
Untreated CF	85.68 ± 2.0	64.60 ± 2.0	25.93	4.63	30.56
CF-GO 0.5	59.25 ± 2.0	50.22 ± 2.0	34.15	15.07	49.22
CF-GO-TCT-DETA 0.1	51.98 ± 2.0	45.37 ± 2.0	36.81	18.23	55.04
CF-GO-TCT-DETA 0.5	41.32 ± 2.0	39.62 ± 2.0	39.80	23.04	62.84
CF-GO-TCT-DETA 1.0	34.69 ± 2.0	33.58 ± 2.0	42.67	25.17	67.78
CF-GO-TCT-DETA 1.5	37.57 ± 2.0	31.34 ± 2.0	43.66	23.20	66.86

enhanced mechanical interlocking of GO with matrix resin [58]. In addition, the chemical bond reactions of amine groups on functionalized GO surface with CF and epoxy resin also presented a positive effect on the interface of CF composite. When the functionalized GO sheets were distributed uniformly on the CF surface, which was conducive to enhance the stress transfer efficiencies and stiffen effectively at the interface area. Whereas, further increasing the GO-TCT-DETA content to 1.5 wt% led to the reduced IFSS owing to the agglomeration of GO-TCT-DETA in the interface area, as verified by Fig. 4f.

The complex interface layer of CF/epoxy composites might be composed of nanoparticles (GO-TCT-DETA) and sizing polymer (epoxy resin), which could effectively present synergistic effects in the integrated interface region and enhance the interfacial interactions. The failure morphologies of debonding regions were observed by SEM, as illustrated in Fig. 5(a-f). The debonding failure surfaces of untreated CF presented a smooth topography without any residual resin. For CF-GO, a little resin remained on the failure surfaces while a big void appeared between CF and resin in Fig. 5b, this manifested that the GO agglomeration might influence the stress transfer. It was noted that with adding the GO-TCT-DETA in sizing, the debonding failure surfaces became rougher, more and more bulges (epoxy fragments and GO sheets) remained on the surface as seen in Fig. 5c–e. This was because that both interfacial bonding (carboxyl-CFs and amino-GO, amino-GO and epoxy) all became too strong to be pulled-out easily, the schematic diagram of interface reactions was illustrated in Fig. 5 (below). Obviously, the GO sheets with good dispersity and chemical activity were highly effective in intensifying the mechanical interlocking and interfacial reaction as well as repressing the crack diffusion at the interface [59].

The ILSS was further employed to testify the effects of sizing agent with GO and GO-TCT-DETA on the interfacial performances in CF/epoxy composites, as presented in Fig. 5. The ILSS of CF/epoxy composites was increased by 100.2% from 35.6 MPa for untreated CFs without sizing to 71.3 MPa (a maximum ILSS) for CFs with GO-TCT-DETA 1.0 sizing. Compared to CFs sized by GO, the introduction of GO-TCT-DETA has made more contribution to the ILSS. It could conclude that the uniformly dispersed GO sheets on CF surfaces could prominently increase the interfacial interactions. Adding nanosheets would affect the interfacial stress transfer. Zhang et al. [60] reported a 27.2% improvement of ILSS in a fiber/epoxy composites when GO modified sizing agent was introduced on the CFs surface. Wu et al. [27] reported that the ILSS of the fiber/methylphenylsilicone resin composites was increased by 46.52% through introducing silanized carbon nanotubes modified sizing agent on the CFs surface. Compared with previous studies, the sizing agent with GO-TCT-DETA on CF reinforced composites had the highest ILSS percentage increased.

3.4.2. *Flexural property of CF/epoxy composites*

The flexural behaviors were evaluated to further study the comprehensive effects of GO and GO-TCT-DETA sizing on CF/epoxy composites, which could mirror the structural features of the modified laminates in response to complicated stress states. The flexural testing results are shown in Fig. 6. It was clearly demonstrated that the GO and GO derivative attachment endowed the hierarchical composites with a higher flexural strength and modulus than the untreated fiber composites. The increase of GO-TCT-DETA content resulted in a gradual improvement of the flexural strength. The CF-GO-TCT-DETA 1.0/epoxy composites exhibited a maximum flexural strength (1202.0 MPa) and modulus (70.3 GPa), with an increase of 78.3% and 77.5% in comparison with untreated CF composites, respectively. Inversely, a further addition of GO-TCT-DETA led to a reduction of flexural properties. The degeneration in the mechanical performances could be due to the exasperation of GO-TCT-DETA dispersibility in interface area.

Basically, the interfacial failure mode of composite includes adhesive and cohesive failure, which depended on the interfacial states [61–63] The SEM images in Fig. 7 show the fracture morphologies of the composites, revealing a prominent difference between the untreated CF and derived GO-reinforced composites. For untreated CF composites, the interface de-bonding between CFs and epoxy was obvious and the

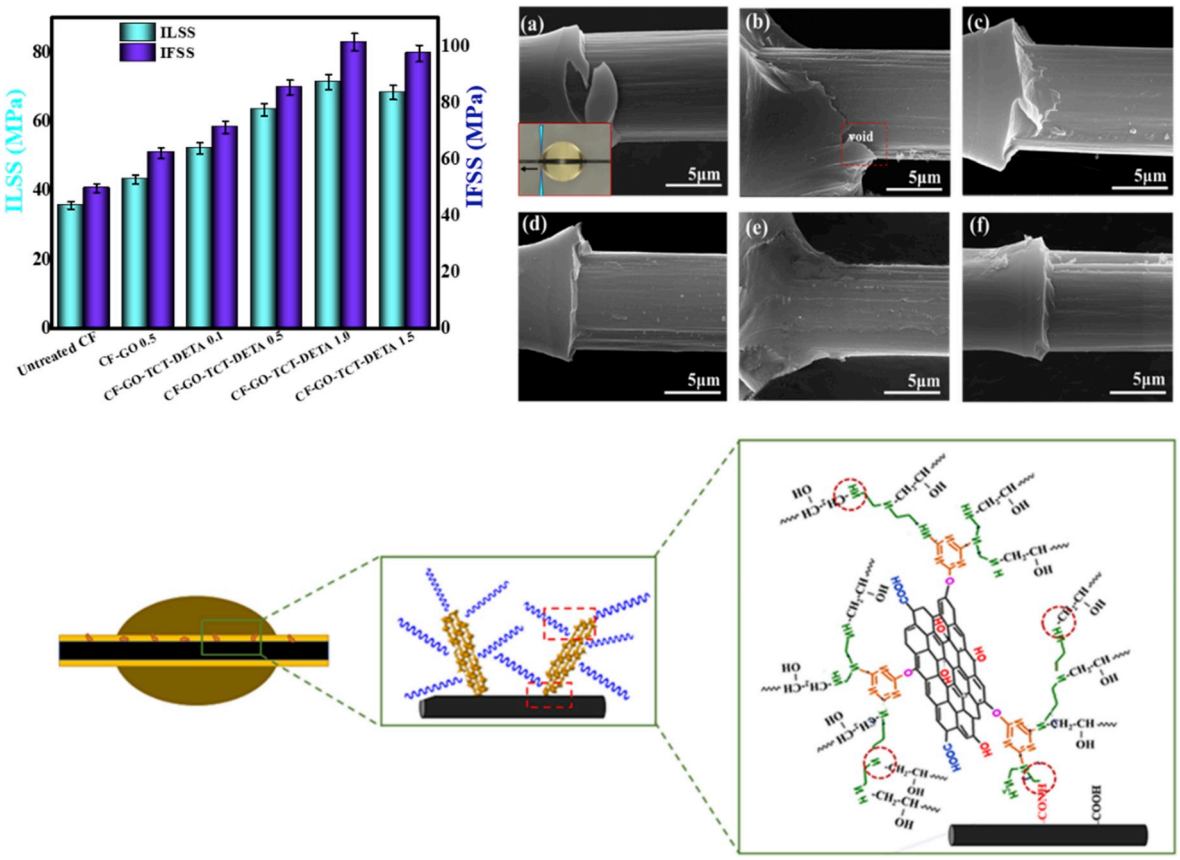

Fig. 5. IFSS and ILSS of CF/epoxy composite and SEM micrographs after de-bonding samples: (a) untreated CFs, (b) CF-GO 0.5, (c) CF-GO-TCT-DETA 0.1, (d) CF-GO-TCT-DETA 0.5, (e) CF-GO-TCT-DETA 1.0 and (f) CF-GO-TCT-DETA 1.5 and Schematic diagrams of interface reaction between CF-GO-TCT-DETA and epoxy (below).

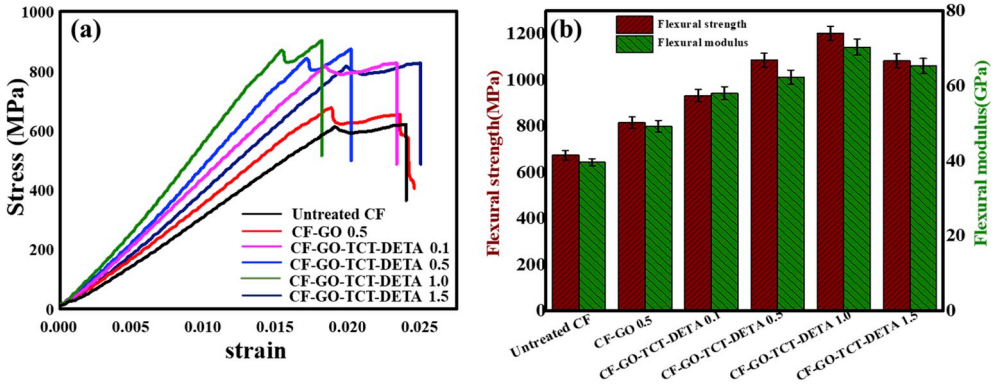

Fig. 6. Flexural properties of composites: (a) Flexural stress-strain curves, (b) Flexural strength and modulus.

pulled-out fibers representatively presented a smooth fracture surface (Fig. 7a). The fracture micromechanism was seen to be principally adhesive failure and the schematic diagrams were displayed in Fig. 7d. While in the CF-GO/epoxy case (Fig. 7b), the CFs surface was not as clean as that of untreated CFs and the extent of pull out was less. Some resin fragments and GO remaining on the CFs surface were traced, the fiber/epoxy debonding was combined with the fiber pull-out and resin/resin debonding (Fig. 7e), manifesting the slight improvement of interfacial adhesion after GO modified sizing treatment. For CF-GO-TCT-DETA 1.0 composites (Fig. 7c), the number of de-bonding fiber decreased and the de-bonding took place in the matrix, which indicated the increased interfacial strength and the distribution state of GO-TCT-DETA in the matrix surrounding CFs. The primary mechanism of fiber/matrix debonding was cohesive failure (Fig. 7f). Moreover, the development of these microstructures would be also related to the enhanced interface layer supplied by GO-TCT-DETA sizing, which was responsible for improving the load transfer between epoxy and CF surfaces [64,65].

4. Conclusions

A brief and efficient approach was used to introduce triazine derivatives functionalized GO onto the CFs surface by sizing process for the CFs/epoxy composites. The TCT-DETA was grafted successfully on the GO surface. The dispersion of GO-TCT-DETA in sizing agent was better than that of virgin GO. An epoxy sizing with different contents of GO-TCT-DETA was deposited onto the CFs surface and the surface roughness increased prominently. The addition of GO-TCT-DETA improved

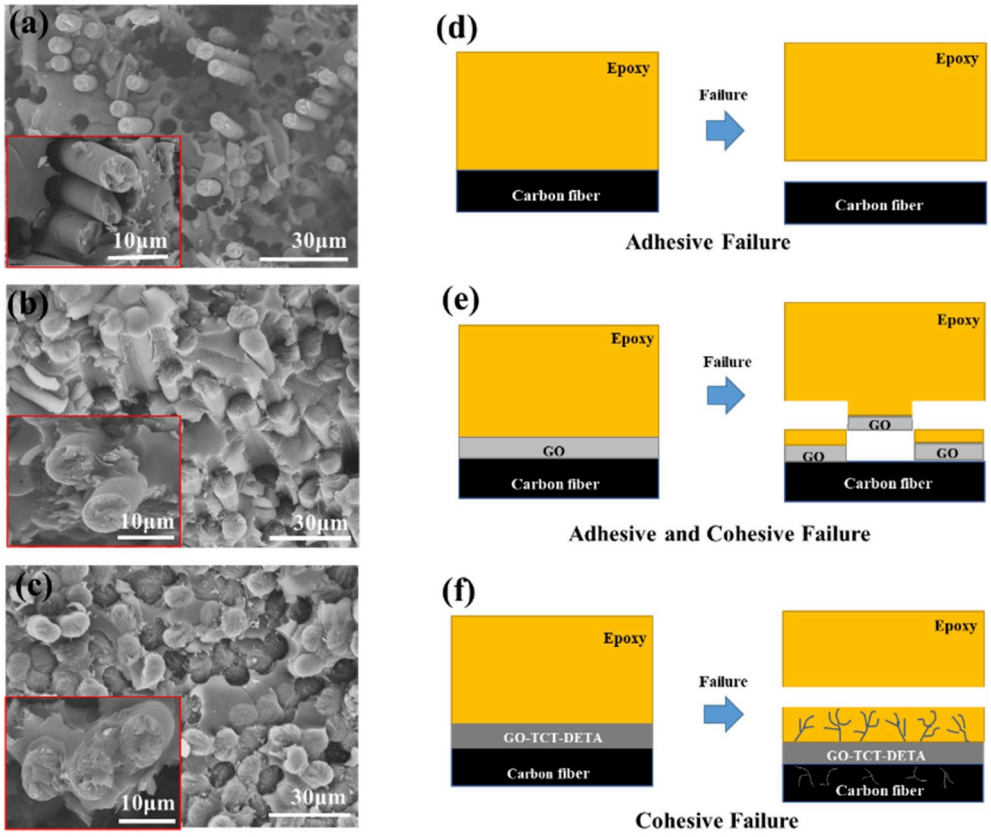

Fig. 7. Micro-morphologies and schematic diagrams of interface failure (a,d) untreated CF composite, (b,e) CF-GO 0.5 composite, (c,f) GO-TCT-DETA 0.5 composite.

effectively the covalent bonding, mechanical interlocking and wettability between CFs and matrix. Furthermore, the nanoscale reinforcing interface containing moderate GO-TCT-DETA could enhance effectively the stress transfer and relieve stress concentrations. The composites reinforced with CF-GO-TCT-DETA 1.0 showed the highest enhancement in the interfacial adhesion, increasing 104.2% and 62.9% in IFSS in comparison to that of untreated CF composites and CF-GO composites, respectively. The flexural properties of CF-GO-TCT-DETA modified CF composites, including flexural strength (1202.0 MPa) and modulus (70.3 GPa), are higher than that of the normal composites (674 MPa and 39.6 GPa). The fibers modified by CF-GO-TCT-DETA without agglomeration exert the highest mechanical properties. Therefore, the presented approach shows a potential for enhancing the interfacial and flexural properties of CFs reinforced composites through using functionalized GO sheets modified fiber sizing for many potential applications including electromagnetic interference (EMI) shielding [66–68], anticorrosion coating [69], catalysis [70], energy [71–73], value-added chemicals from wastes [74], unique coating [54,75], and potential electronics [76,77].

Acknowledgement

This work was supported by the project of Natural Science Foundation of China (NO. 51803102), Project of China Postdoctoral Science Foundation (No. 2017M612196 and No. 2017M612197).

References

[1] Shirvanimoghaddam K, Hamim SU, Karbalaei Akbari M, Fakhrhoseini SM, Khayyam H, Pakseresht AH, Ghasali E, Zabet M, Munir KS, Jia S, Davim JP, Naebe M. Carbon fiber reinforced metal matrix composites: fabrication processes and properties. Compos Appl Sci Manuf 2017;92:70–96.

[2] Ma L, Zhu Y, Wang M, Yang X, Song G, Huang Y. Enhancing interfacial strength of epoxy resin composites via evolving hyperbranched amino-terminated POSS on carbon fiber surface. Compos Sci Technol 2019;170:148–56.

[3] Ma L, Li N, Wu G, Song G, Li X, Han P, Wang G, Huang Y. Interfacial enhancement of carbon fiber composites by growing TiO_2 nanowires onto amine-based functionalized carbon fiber surface in supercritical water. Appl Surf Sci 2018;433:560–7.

[4] Zhao Z, Bai P, Misra RDK, Dong M, Guan R, Li Y, Zhang J, Tan L, Gao J, Ding T, Du W, Guo Z. AlSi10Mg alloy nanocomposites reinforced with aluminum-coated graphene: selective laser melting, interfacial microstructure and property analysis. J Alloy Comp 2019;792:203–14.

[5] Sun H, Yang Z, Pu Y, Dou W, Wang C, Wang W, Hao X, Chen S, Shao Q, Dong M, Wu S, Ding T, Guo Z. Zinc oxide/vanadium pentoxide heterostructures with enhanced day-night antibacterial activities. J Colloid Interface Sci 2019;547:40–9.

[6] Lin B, Lin Z, Chen S, Yu M, Li W, Gao Q, Dong M, Shao Q, Wu S, Ding T, Guo Z. Surface intercalated spherical MoS2xSe2(1-x) nanocatalysts for highly efficient and durable hydrogen evolution reactions. Dalton Trans 2019. https://doi.org/10.1039/c9dt01218d.

[7] Lin Z, Lin B, Wang Z, Chen S, Wang C, Dong M, Gao Q, Shao Q, Ding T, Liu H, Wu S, Guo Z. Facile Preparation of 1T/2H-Mo($S_{1-x}Se_x$)$_2$ nanoparticles for boosting hydrogen evolution reaction. ChemCatChem 2019;11(8):2217–22.

[8] Le K, Wang Z, Wang F, Wang Q, Shao Q, Murugadoss V, Wu S, Liu W, Liu J, Gao Q, Guo Z. Sandwich-like NiCo layered double hydroxide/reduced graphene oxide nanocomposite cathodes for high energy density asymmetric supercapacitors. Dalton Trans 2019;48(16):5193–202.

[9] Li R, Zhu X, Fu Q, Liang G, Chen Y, Luo L, Dong M, Shao Q, Lin C, Wei R, Guo Z. Nanosheet-based Nb12O29 hierarchical microspheres for enhanced lithium storage. Chem Commun 2019;55(17):2493–6.

[10] Idrees M, Batool S, Kong J, Zhuang Q, Liu H, Shao Q, Lu N, Feng Y, Wujcik EK, Gao Q, Ding T, Wei R, Guo Z. Polyborosilazane derived ceramics - nitrogen sulfur dual doped graphene nanocomposite anode for enhanced lithium ion batteries. Electrochim Acta 2019;296:925–37.

[11] Wang C, Lan F, He Z, Xie X, Zhao Y, Hou H, Guo L, Murugadoss V, Liu H, Shao Q, Gao Q, Ding T, Wei R, Guo Z. Iridium-based catalysts for solid polymer electrolyte electrocatalytic water splitting. ChemSusChem 2019;12(8):1576–90.

[12] Zhao Y, Wang S, Zhang B, Yuan Y, Guo Q, Hou H. The anisotropy of three-component medium entropy alloys in AlCoCrFeNi system: first-principle studies. J Solid State Chem 2019;276:232–7.

[13] Shen C, Liu X, Cao H, Zhou Y, Liu J, Tang J, Guo X, Huang H, Chen X. Brain-Like navigation scheme based on MEMS-INS and place recognition. Appl Sci 2019;9(8):1708.

[14] Liu L, Yan F, Li M, Zhang M, Xiao L, Shang L, Ao Y. A novel thermoplastic sizing containing graphene oxide functionalized with structural analogs of matrix for

improving interfacial adhesion of CF/PES composites. Compos Appl Sci Manuf 2018;114:418–28.
[15] Wu G, Chen L, Liu L. Effects of silanization and silica enrichment of carbon fibers on interfacial properties of methylphenylsilicone resin composites. Compos Appl Sci Manuf 2017;98:159–65.
[16] Liang T, Qi L, Ma Z, Xiao Z, Wang Y, Liu H, Zhang J, Guo Z, Liu C, Xie W, Ding T, Lu N. Experimental study on thermal expansion coefficient of composite multi-layered flaky gun propellants. Compos B Eng 2019;166:428–35.
[17] Zhao G, Hu P, Zhou S, Chen G, An Y, Cheng Y, An J, Zhang X, Han W. Ordered silica nanoparticles grown on a three-dimensional carbon fiber architecture substrate with siliconborocarbonitride ceramic as a thermal barrier coating. ACS Appl Mater Interfaces 2016;8(6):4216–25.
[18] Ma R, Wang Y, Qi H, Shi C, Wei G, Xiao L, Huang Z, Liu S, Yu H, Teng C, Liu H, Murugadoss V, Zhang J, Wang Y, Guo Z. Nanocomposite sponges of sodium alginate/graphene oxide/polyvinyl alcohol as potential wound dressing: in vitro and in vivo evaluation. Compos B Eng 2019;167:396–405.
[19] Wu G, Ma L, Jiang H, Liu L, Huang Y. Improving the interfacial strength of silicone resin composites by chemically grafting silica nanoparticles on carbon fiber. Compos Sci Technol 2017;153:160–7.
[20] Zhao M, Meng L, Ma L, Ma L, Yang X, Huang Y, Ryu JE, Shankar A, Li T, Yan C, Guo Z. Layer-by-layer grafting CNTs onto carbon fibers surface for enhancing the interfacial properties of epoxy resin composites. Compos Sci Technol 2018;154:28–36.
[21] Gu H, Zhang H, Ma C, Sun H, Liu C, Dai K, Zhang J, Wei R, Ding T, Guo Z. Smart strain sensing organic–inorganic hybrid hydrogels with nano barium ferrite as the cross-linker. J Mater Chem C 2019;7(8):2353–60.
[22] Wu Z, Cui H, Chen L, Jiang D, Weng L, Ma Y, Li X, Zhang X, Liu H, Wang N, Zhang J, Ma Y, Zhang M, Huang Y, Guo Z. Interfacially reinforced unsaturated polyester carbon fiber composites with a vinyl ester-carbon nanotubes sizing agent. Compos Sci Technol 2018;164:195–203.
[23] Wu ZJ, Gao S, Chen L, Jiang DW, Shao Q, Zhang B, Zhai ZH, Wang C, Zhao M, Ma YY, Zhang XH, Weng L, Zhang MY, Guo ZH. Electrically insulated epoxy nanocomposites reinforced with synergistic core-shell SiO_2@MWCNTs and montmorillonite bifillers. Macromol Chem Phys 2017;218(23).
[24] He Y, Yang S, Liu H, Shao Q, Chen Q, Lu C, Jiang Y, Liu C, Guo Z. Reinforced carbon fiber laminates with oriented carbon nanotube epoxy nanocomposites: magnetic field assisted alignment and cryogenic temperature mechanical properties. J Colloid Interface Sci 2018;517:40–51.
[25] He Y, Chen Q, Yang S, Lu C, Feng M, Jiang Y, Cao G, Zhang J, Liu C. Micro-crack behavior of carbon fiber reinforced Fe3O4/graphene oxide modified epoxy composites for cryogenic application. Compos Appl Sci Manuf 2018;108:12–22.
[26] Rahmanian S, Suraya AR, Zahari R, Zainudin ES. Synthesis of vertically aligned carbon nanotubes on carbon fiber. Appl Surf Sci 2013;271:424–8.
[27] Wu G, Ma L, Liu L, Wang Y, Xie F, Zhong Z, Zhao M, Jiang B, Huang Y. Interfacially reinforced methylphenylsilicone resin composites by chemically grafting multiwall carbon nanotubes onto carbon fibers. Compos B Eng 2015;82:50–8.
[28] Shi L, Ma L, Li P, Wang M, Guo S, Han P, Song G. The effect of self-synthesized hydroxyl-terminated hyperbranched polymer interface layer on the properties of carbon fiber reinforced epoxy composites. Appl Surf Sci 2019;479:334–43.
[29] Zhang S, Liu WB, Hao LF, Jiao WC, Yang F, Wang RG. Preparation of carbon nanotube/carbon fiber hybrid fiber by combining electrophoretic deposition and sizing process for enhancing interfacial strength in carbon fiber composites. Compos Sci Technol 2013;88:120–5.
[30] Wang C, Li J, Sun S, Li X, Zhao F, Jiang B, Huang Y. Electrophoretic deposition of graphene oxide on continuous carbon fibers for reinforcement of both tensile and interfacial strength. Compos Sci Technol 2016;135:46–53.
[31] Chen J, Wang K, Zhao Y. Enhanced interfacial interactions of carbon fiber reinforced PEEK composites by regulating PEI and graphene oxide complex sizing at the interface. Compos Sci Technol 2018;154:175–86.
[32] Wang SL, Yu XQ, Zhang YF. Large-scale fabrication of translucent, stretchable and durable superhydrophobic composite films. J Mater Chem A 2017;5(45):23489–96.
[33] Wu G, Ma L, Liu L, Wang Y, Xie F, Zhong Z, Zhao M, Jiang B, Huang Y. Interface enhancement of carbon fiber reinforced methylphenylsilicone resin composites modified with silanized carbon nanotubes. Mater Des 2016;89:1343–9.
[34] Ma Y, Yan C, Xu H, Liu D, Shi P, Zhu Y, Liu J. Enhanced interfacial properties of carbon fiber reinforced polyamide 6 composites by grafting graphene oxide onto fiber surface. Appl Surf Sci 2018;452:286–98.
[35] Yao X, Gao X, Jiang J, Xu C, Deng C, Wang J. Comparison of carbon nanotubes and graphene oxide coated carbon fiber for improving the interfacial properties of carbon fiber/epoxy composites. Compos B Eng 2018;132:170–7.
[36] Feng Z-Q, Wu F, Jin L, Wang T, Dong W, Zheng J. Graphene nanofibrous foam designed as an efficient oil absorbent. Ind Eng Chem Res 2019;58(8):3000–8.
[37] Ma J, Sun Y, Zhang M, Yang M, Gong X, Yu F, Zheng J. Comparative study of graphene hydrogels and aerogels reveals the important role of buried water in pollutant adsorption. Environ Sci Technol 2017;51(21):12283–92.
[38] Ma J, Shen W, Li C, Zheng J, Yu F. Graphene cryogel-based counter electrode materials freeze-dried using different solution media for dye-sensitized solar cells. Chem Eng J 2017;319:155–62.
[39] Li J, Ma J, Chen S, Huang Y, He J. Adsorption of lysozyme by alginate/graphene oxide composite beads with enhanced stability and mechanical property. Mater Sci Eng C Mater Biol Appl 2018;89:25–32.
[40] Guo S, Ma L, Song G, Li X, Li P, Wang M, Shi L, Gu Z, Huang Y. Covalent grafting of triazine derivatives onto graphene oxide for preparation of epoxy composites with improved interfacial and mechanical properties. J Mater Sci 2018;53(24):16318–30.
[41] Guan L-Z, Wan Y-J, Gong L-X, Yan D, Tang L-C, Wu L-B, Jiang J-X, Lai G-Q. Toward effective and tunable interphases in graphene oxide/epoxy composites by grafting different chain lengths of polyetheramine onto graphene oxide. J Mater Chem A 2014;2(36):15058–69.
[42] Meng L, Fan D, Huang Y, Jiang Z, Zhang C. Comparison studies of surface cleaning methods for PAN-based carbon fibers with acetone, supercritical acetone and subcritical alkali aqueous solutions. Appl Surf Sci 2012;261:415–21.
[43] Luo J, Yang S, Lei L, Zhao J, Tong Z. Toughening, synergistic fire retardation and water resistance of polydimethylsiloxane grafted graphene oxide to epoxy nanocomposites with trace phosphorus. Compos Appl Sci Manuf 2017;100:275–84.
[44] Schaubroeck D, De Baets J, Desmet T, Dubruel P, Schacht E, Van Vaeck L, Van Calster A. Surface modification of an epoxy resin with polyamines via cyanuric chloride coupling. Appl Surf Sci 2010;256(21):6269–78.
[45] Ma LC, Wu GS, Zhao M, Li XR, Han P, Song GJ. Modification of carbon fibers surfaces with polyetheramines: the role of interphase microstructure on adhesion properties of CF/epoxy composites. Polym Compos 2018;39:E2346–55.
[46] Xu G, Shi Z, Zhao Y, Deng J, Dong M, Liu C, Murugadoss V, Mai X, Guo Z. Structural characterization of lignin and its carbohydrate complexes isolated from bamboo (Dendrocalamus sinicus). Int J Biol Macromol 2019;126:376–84.
[47] Shi Z, Jia C, Wang D, Deng J, Xu G, Wu C, Dong M, Guo Z. Synthesis and characterization of porous tree gum grafted copolymer derived from Prunus cerasifera gum polysaccharide. Int J Biol Macromol 2019;133:964–70.
[48] Jiang D, Wang Y, Li B, Sun C, Wu Z, Yan H, Xing L, Qi S, Li Y, Liu H, Xie W, Wang X, Ding T, Guo Z. Flexible sandwich structural strain sensor based on silver nanowires decorated with self-healing substrate. Macromol Mater Eng 2019;0(0):1900074.
[49] Shi ZJ, Wu CH, Wu Y, Liu HQ, Xu GF, Deng J, Gu HB, Liu H, Zhang JX, Umar A, Ma Y, Guo ZH. Optimization of epoxypinane synthesis by silicotungstic acid supported on SBA-15 catalyst using response surface methodology. Sci Adv Mater 2019;11(5):699–707.
[50] Shi Z, Wu C, Gu Y, Liang Y, Xu G, Liu H, Zhang J, Hou H, Zhang J, Guo Z. Preparation and characterization of mesoporous CuO/ZSM-5 catalysts for automotive exhaust purification. Sci Adv Mater 2019. https://doi.org/10.1166/sam.2019.3559 (in press).
[51] Yang J, Yang W, Wang X, Dong M, Liu H, Wujcik EK, Shao Q, Wu S, Ding T, Guo Z. Synergistically toughening polyoxymethylene by methyl methacrylate–butadiene–styrene copolymer and thermoplastic polyurethane. Macromol Chem Phys 2019;0(0):1800567.
[52] Gu H, Xu X, Dong M, Xie P, Shao Q, Fan R, Liu C, Wu S, Wei R, Guo Z. Carbon nanospheres induced high negative permittivity in nanosilver-polydopamine metacomposites. Carbon 2019;147:550–8.
[53] Gong X, Liu Y, Wang Y, Xie Z, Dong Q, Dong M, Liu H, Shao Q, Lu N, Murugadoss V, Ding T, Guo Z. Amino graphene oxide/dopamine modified aramid fibers: preparation, epoxy nanocomposites and property analysis. Polymer 2019;168:131–7.
[54] Wang W, Hao X, Chen S, Yang Z, Wang C, Yan R, Zhang X, Liu H, Shao Q, Guo Z. pH-responsive Capsaicin@chitosan nanocapsules for antibiofouling in marine applications. Polymer 2018;158:223–30.
[55] Gao B, Zhang J, Hao Z, Huo L, Zhang R, Shao L. In-situ modification of carbon fibers with hyperbranched polyglycerol via anionic ring-opening polymerization for use in high-performance composites. Carbon 2017;123:548–57.
[56] Zhao M, Meng L, Ma L, Wu G, Xie F, Ma L, Wang W, Jiang B, Huang Y. Stepwise growth of melamine-based dendrimers onto carbon fibers and the effects on interfacial properties of epoxy composites. Compos Sci Technol 2017;138:144–50.
[57] Wang C, Chen L, Li J, Sun S, Ma L, Wu G, Zhao F, Jiang B, Huang Y. Enhancing the interfacial strength of carbon fiber reinforced epoxy composites by green grafting of poly(oxypropylene) diamines. Compos Appl Sci Manuf 2017;99:58–64.
[58] Zhang C, Wu G, Jiang H. Tuning interfacial strength of silicone resin composites by varying the grafting density of octamaleamic acid-POSS modified onto carbon fiber. Compos Appl Sci Manuf 2018;109:555–63.
[59] Li N, Zong L, Wu Z, Liu C, Wang J, Jian X. Effect of Poly(phthalazinone ether ketone) with amino groups on the interfacial performance of carbon fibers reinforced PPBES resin. Compos Sci Technol 2017;149:178–84.
[60] Zhang Q, Jiang D, Liu L, Huang Y, Long J, Wu G, Wu Z, Umar A, Guo J, Zhang X, Guo Z. Effects of graphene oxide modified sizing agents on interfacial properties of carbon fibers/epoxy composites. J Nanosci Nanotechnol 2015;15(12):9807–11.
[61] Peng Q, Li Y, He X, Lv H, Hu P, Shang Y, Wang C, Wang R, Sritharan T, Du S. Interfacial enhancement of carbon fiber composites by poly(amido amine) functionalization. Compos Sci Technol 2013;74:37–42.
[62] Liu L, Yan F, Li M, Zhang M, Xiao L, Shang L, Ao Y. Improving interfacial properties of hierarchical reinforcement carbon fibers modified by graphene oxide with different bonding types. Compos Appl Sci Manuf 2018;107:616–25.
[63] Liu L, Yan F, Li M, Zhang M, Xiao L, Ao Y. Self-assembly of graphene aerogel on carbon fiber for improvement of interfacial properties with epoxy resin. Mater Lett 2018;218:44–6.
[64] Servinis L, Beggs KM, Scheffler C, Wölfel E, Randall JD, Gengenbach TR, Demir B, Walsh TR, Doeven EH, Francis PS, Henderson LC. Electrochemical surface modification of carbon fibres by grafting of amine, carboxylic and lipophilic amide groups. Carbon 2017;118:393–403.
[65] Gao B, Zhang R, He M, Wang C, Liu L, Zhao L, Wen Z, Ding Z. Interfacial microstructure and mechanical properties of carbon fiber composites by fiber surface modification with poly(amidoamine)/polyhedral oligomeric silsesquioxane. Compos Appl Sci Manuf 2016;90:653–61.
[66] Jiang D, Murugadoss V, Wang Y, Lin J, Ding T, Wang Z, Shao Q, Wang C, Liu H, Lu N, Wei R, Subramania A, Guo Z. Electromagnetic interference shielding polymers and nanocomposites-a review. Polym Rev 2019;59(2):280–337.

[67] Wang C, Murugadoss V, Kong J, He Z, Mai X, Shao Q, Chen Y, Guo L, Liu C, Angaiah S, Guo Z. Overview of carbon nanostructures and nanocomposites for electromagnetic wave shielding. Carbon 2018;140:696–733.
[68] Wu N, Xu D, Wang Z, Wang F, Liu J, Liu W, Shao Q, Liu H, Gao Q, Guo Z. Achieving superior electromagnetic wave absorbers through the novel metal-organic frameworks derived magnetic porous carbon nanorods. Carbon 2019;145:433–44.
[69] Zhu G, Cui X, Zhang Y, Chen S, Dong M, Liu H, Shao Q, Ding T, Wu S, Guo Z. Poly (vinyl butyral)/Graphene oxide/poly (methylhydrosiloxane) nanocomposite coating for improved aluminum alloy anticorrosion. Polymer 2019;172:415–22.
[70] Chen Q, Yin Q, Dong A, Gao Y, Qian Y, Wang D, Dong M, Shao Q, Liu H, Han B-H, Ding T, Guo Z, Wang N. Metal complex hybrid composites based on fullerene-bearing porous polycarbazole for H2, CO2 and CH4 uptake and heterogeneous hydrogenation catalysis. Polymer 2019;169:255–62.
[71] Liu M, Li B, Zhou H, Chen C, Liu Y, Liu T. Extraordinary rate capability achieved by a 3D "skeleton/skin" carbon aerogel–polyaniline hybrid with vertically aligned pores. Chem Commun 2017;53(19):2810–3.
[72] Hou C, Wang J, Du W, Wang J, Du Y, Liu C, Zhang J-x, Hou H, Dang F, Zhao L, Guo Z. One-pot synthesized molybdenum dioxide-molybdenum carbide heterostructures coupled with 3D holey carbon nanosheets for highly efficient and ultrastable cycling lithium-ion storage. J Mater Chem A 2019. https://doi.org/10.1039/c9ta03551f.
[73] Kirubasankar B, Murugadoss V, Lin J, Ding T, Dong M, Liu H, Zhang J, Li T, Wang N, Guo Z, Angaiah S. In situ grown nickel selenide on graphene nanohybrid electrodes for high energy density asymmetric supercapacitors. Nanoscale 2018;10 (43):20414–25.
[74] Hu Q, Zhou N, Gong K, Liu H, Liu Q, Sun D, Wang Q, Shao Q, Liu H, Qiu B, Guo Z. Intracellular polymer substances induced conductive polyaniline for improved methane production from anaerobic wastewater treatment. ACS Sustainable Chem Eng 2019;7(6):5912–20.
[75] Cui X, Zhu G, Pan Y, Shao Q, Zhao C, Dong M, Zhang Y, Guo Z. Polydimethylsiloxane-titania nanocomposite coating: fabrication and corrosion resistance. Polymer 2018;138:203–10.
[76] Berndt AJ, Hwang J, Islam MD, Sihn A, Urbas AM, Ku Z, Lee SJ, Czaplewski DA, Dong M, Shao Q, Wu S, Guo Z, Ryu JE. Poly(sulfur-random-(1,3-diisopropenylbenzene)) based mid-wavelength infrared polarizer: optical property experimental and theoretical analysis. Polymer 2019. https://doi.org/10.1016/j.polymer.2019.05.036.
[77] Qi H, Teng M, Liu M, Liu S, Li J, Yu H, Teng C, Huang Z, Liu H, Shao Q, Umar A, Ding T, Gao Q, Guo Z. Biomass-derived nitrogen-doped carbon quantum dots: highly selective fluorescent probe for detecting Fe^{3+} ions and tetracyclines. J Colloid Interface Sci 2019;539:332–41.